ACS Catalysis

Research Article

pubs.acs.org/acscatalysis

pH Effect on Electrochemistry of Nitrogen-Doped Carbon Catalyst for Oxygen Reduction Reaction

Kai Wan,[†] Zhi-peng Yu,[†] Xiao-hua Li,[†] Ming-yao Liu,[†] Gang Yang,[†] Jin-hua Piao,[‡] and Zhen-xing Liang*[,†,§]

[†]Key Laboratory on Fuel Cell Technology of Guangdong Province, School of Chemistry and Chemical Engineering, [‡]School of Light Industry and Food Science, South China University of Technology, Guangzhou 510641, People's Republic of China

[§]Center for Electrochemistry, Department of Chemistry, The University of Texas at Austin, Austin, Texas 78712, United States

Supporting Information

ABSTRACT: In this work, the effect of pH on a nitrogen-doped ordered mesoporous carbon catalyst for the oxygen reduction reaction (ORR) is extensively investigated. Electrochemical methods, including cyclic voltammetry (CV), rotating ring-disk electrode (RRDE), and cathodic stripping voltammetry, are applied to investigate the electrochemical behavior in electrolyte solutions of different pHs (0−2, 7, 12−14). The CV result reveals that nitrogen-doped carbon has a variety of enriched reversible redox couples on the surface, and the pH has a significant effect. Whether these redox couples are electrochemically active or inactive to the ORR depends on the electrolyte used. In acid media, an oxygen molecule directly interacts with the redox couple, and its reduction proceeds by the surface-confined redox-mediation mechanism, yielding water as the product. Similarly, the first electron transfer in alkaline media is achieved by the surface-confined redox-mediation mechanism at the higher potentials. With decreasing potential, another parallel charge transfer process by the outer-sphere electron transfer mechanism gets pronounced, followed by parallel 2-e and 4-e reduction of oxygen. The proposed mechanisms are well supported by the following electrochemical results. At high potentials, the Tafel slope remains unchanged (60−70 mV dec^{-1}) at all investigated pHs, and the reaction order of proton and hydroxyl ions is found to be 1 and −0.5, respectively, in acid and alkaline media. The electron transfer number is ∼4 at high potentials in both acid and alkaline media; however, at higher pHs, it shows a considerable decrease as the potential decreases, indicating the change in the reaction pathway. Finally, the nitrogen-doped carbon catalyst shows performance in alkaline media superior to that in acid media. Such a gap in performance is rationalized by considering the chemical change in the surface at different pH values.

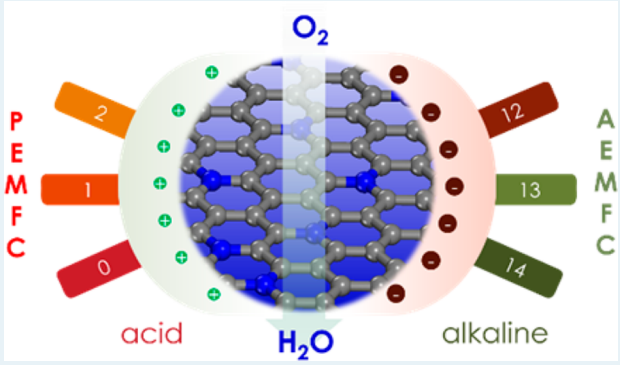

KEYWORDS: *active site, electrocatalytic activity, nitrogen-doped carbon, ordered mesoporous carbon, oxygen reduction reaction, pH effect*

1. INTRODUCTION

The high cost and source scarcity of platinum pose a great challenge to the commercialization of fuel cell technology.[1−5] Nitrogen-doped carbon materials have been regarded as one of the most promising Pt-alternative catalysts and have aroused increasing interest in the past decade.[6−13] For example, Dai[3] synthesized 1-D nitrogen-doped carbon nanotubes (CNT), which yielded catalytic activity to the oxygen reduction reaction (ORR) superior to that for Pt in alkaline media. Bao[14] developed a 2-D nitrogen-doped graphene electrocatalyst that featured high-density active sites and, thus, a decent performance. A novel nanostructure, a 1-D nanotube/2-D graphene complex, was recently developed and proved to be highly active for the ORR.[15] To further increase the volumetric density of active sites, Dodelet[16] synthesized a highly porous carbon catalyst by using a zeolitic imidazolate framework as the precursor, which showed a surprisingly high power density of 0.75 W cm^{-2} at 0.6 V.

In comparison, in fundamental research, the mechanism of the ORR has not been fully understood yet. Both theoretical and experimental findings on the chemical nature of the active sites and rate-determining step (r.d.s.) are often contradictory. Some researchers argue that the nitrogen-adjacent carbon atoms are positively charged and act as the active sites to adsorb the oxygen molecules.[3,14,17,18] Others claim that the first electron may be transferred into solvated oxygen at the outer-Helmholtz plane (OHP) before the adsorption of oxygen.[19,20] In addition, some researchers insist that the transition metal

Received: February 23, 2015
Published: June 1, 2015

DOI: 10.1021/acscatal.5b01089
ACS Catal. 2015, 5, 4325−4332

ions are involved in forming the active sites, on which the oxygen molecule is directly adsorbed and activated.[4,5,15,20,21]

Despite these disputes, it is well documented that the doped carbon catalyst yields an excellent activity to the ORR in alkaline media; however, the activity is rather low in acid media, which prevents its real application in proton exchange membrane fuel cells. The big gap between the acid and alkaline media needs to be explicitly clarified. Mukerjee[20] investigated the effect of pH on the redox potential of the transition metal iron, which is suggested to constitute the active sites; however, the effect on the electrochemical activity was not well addressed.[22] Li[23] found that the protonation of the phenazine moiety in a metal-free graphene catalyst seriously degrades its activity for the ORR. Popov[24] held the same conclusion that the protonation of the nitrogen-doped carbon catalyst degrades the electrocatalytic activity. Dodelet[25] studied the ORR activity of their Fe/N/C catalyst in 0.10 M KOH and 0.10 M $HClO_4$ solutions, and found that the activity is 7−10 times higher at pH = 13 than pH = 1. They[26] further suggested that the lower electrocatalytic activity in acid can be attributed to the protonation of the surface nitrogen groups and the subsequent anion binding.

To the best of our knowledge, the pH effect on the electrochemical behavior of the nitrogen-doped carbon catalyst has been rarely investigated, and the big performance gap in acid and alkaline media has not been well understood. The lack of understanding bottle-necks the efforts to explore novel high-performance electrocatalysts. As such, we investigated the effect of the solution composition on the electrochemical behavior of the nitrogen-doped carbon catalyst in a wide pH window. The findings can both deepen the fundamental understanding on the electrochemical reduction reaction of oxygen and guide the development of novel electrode materials.

2. EXPERIMENTAL SECTION

2.1. Materials Synthesis. The nitrogen-doped ordered mesoporous carbon material was synthesized by a modified nanocasting method.[27] The process is briefly described as follows. (i) Synthesis of SBA-15 template: An aqueous mixture, consisting of Pluronic P123, HCl, and tetraethoxysilane, was stirred for 20 h at 35 °C and then hydrothermally treated at 100 °C for 24 h. The resultant powders were calcined in air at 550 °C for 6 h, and SBA-15 was finally obtained. (ii) Impregnation of the carbon precursor: Pyrrole was impregnated into SBA-15 by the vaporization−capillary condensation method,[27] then the monomer was polymerized upon adding the oxidizing agent $FeCl_3$. (iii) Pyrolysis and template removal: The resultant powders were then subjected to the pyrolysis at 900 °C for 3 h in argon. Finally, the carbon catalyst was obtained by removing the silicate template by boiling in a concentrated NaOH solution.

2.2. Electrochemical Characterization. The electrochemical behavior of the catalyst was characterized by cyclic voltammetry (CV) and linear sweeping voltammetry (LSV) using a three-electrode cell with an electrochemical workstation Zennium (Zahner) at room temperature (25 °C). A platinum wire and a double junction Ag/AgCl reference electrode were used as the counter and reference electrodes, respectively. The working electrode was a rotating ring-disk electrode (glassy carbon disk, 5.0 mm in diameter; platinum ring, 6.5 mm i.d. and 7.5 mm o.d., RRDE). The thin-film electrode on the disk was prepared as follows. Ten milligrams of the catalyst was dispersed in 1.0 mL of Nafion/ethanol (0.84 wt % Nafion) by sonication for 120 min, then 10 μL of the dispersion was transferred onto the glassy carbon disk by using a pipet, yielding the catalyst loading of 0.50 mg cm^{-2}. For comparison reasons, we also measured the electrocatalytic activity for the ORR of the commercially available 40 wt % Pt/C catalyst (HiSPEC4000, Johnson Matthey) with a metal loading of 20 μg cm^{-2}.

The electrolyte solution was first bubbled with argon for 60 min, then a CV test was conducted at 20 mV s^{-1} at the potential range between 0 and 1.23 V (vs reversible hydrogen electrode, RHE) for 20 cycles. If not specified, the LSV curve was collected by scanning the disk potential from 1.2 to 0 V at 5 mV s^{-1} in an oxygen-saturated electrolyte solution under 1600 rpm, from which the ORR polarization curve was extracted by subtracting the capacitive current. During the collection, the potential of the ring was set to be 0.5 V (vs RHE) in alkaline and 1.2 V (vs RHE) in acid to determine the yield of hydrogen peroxide.

The oxygen stripping experiments were done as follows: First, the electrode was conditioned at 1.05 V (vs RHE) for 30 min in argon-saturated 0.10 M KOH solution. The background LSV was then collected by negatively scanning the potential from 1.05 to 0 V at 5 mV s^{-1}. Second, to collect the oxygen-stripping curve, the electrode was conditioned at 1.05 V for 30 min in oxygen-saturated solution, then the gas was switched to argon to purge out the dissolved oxygen in the bulk solution while keeping the electrode potential at 1.05 V. Finally, the oxygen-stripping curve was collected by negatively scanning the potential from 1.05 to 0 V. The same process was repeated to collect the oxygen-stripping curve in 0.10 M $HClO_4$ solution, except that the conditioning potential was set at 1.0 V. The details for selecting the conditioning potential can be found in the Supporting Information.

The pH value was 13.80, 12.89, 11.85, 2.03, 1.05, and 0.13 for 1.0 M KOH, 0.10 KOH, 0.010 M KOH, 0.010 M $HClO_4$, 0.10 M $HClO_4$, 1.0 M $HClO_4$ solutions, respectively.

2.3. Analysis of Kinetics Current and Electron Transfer Number. The kinetics current (i_k) is extracted from the RDE results on the basis of the following Koutecky−Levich equation:

$$\frac{1}{i} = \frac{1}{i_k} + \frac{1}{0.62nFAD^{2/3}\nu^{-1/6}C}\frac{1}{\omega^{1/2}} \quad (1)$$

where n is the electron transfer number, F is the Faradaic constant, A is the electrode area, D is the diffusion coefficient of oxygen in the solution, ν is the solution viscosity, C is the saturated concentration of oxygen, and ω is the angular rotation rate.

The electron transfer number (n) and hydrogen peroxide yield (H_2O_2%) are obtained from the following equations:

$$n = \frac{4|i_d|}{|i_d| + i_r/N} \quad (2)$$

$$H_2O_2(\%) = \frac{2i_r/N}{|i_d| + i_r/N} \times 100\% \quad (3)$$

where i_d is the disk current, i_r is the ring current, and N is the collection efficiency (= 20.50%).

3. RESULTS AND DISCUSSION

3.1. CV at pH = 1, 7, 13. Figure 1 shows the CV curves of the carbon catalyst in acid, neutral, and alkaline media. It is seen

DOI: 10.1021/acscatal.5b01089
ACS Catal. 2015, 5, 4325−4332

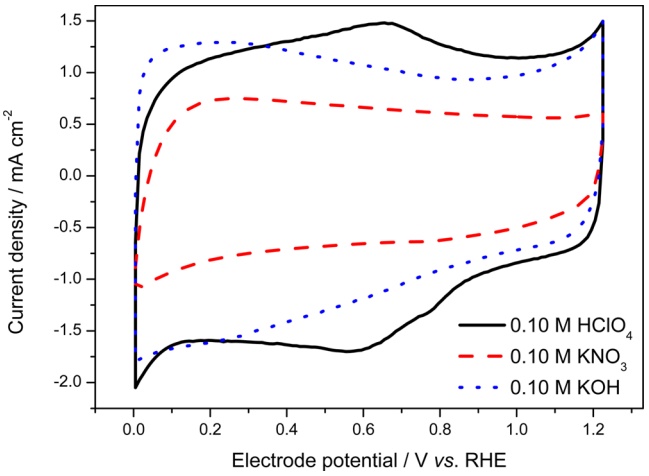

Figure 1. Cyclic voltammetry curves of the catalyst in different electrolytes: 0.10 M $HClO_4$, 0.10 KNO_3, and 0.10 KOH.

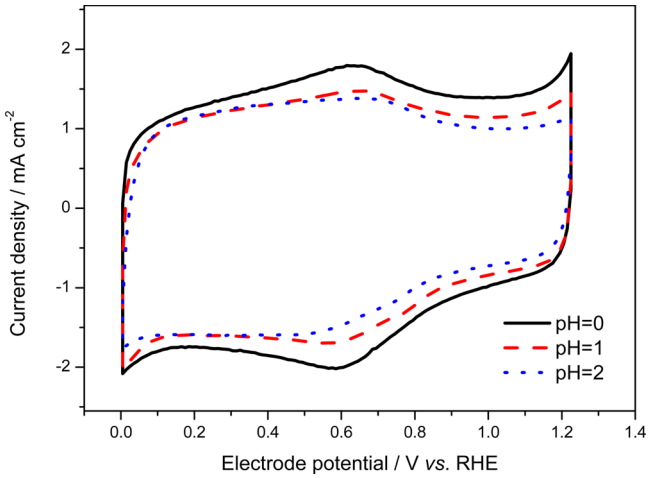

Figure 2. Cyclic voltammetry curves of the catalyst in $HClO_4$ solutions of three concentrations: 1.0, 0.10, and 0.010 M.

that the catalyst shows different features at the three pH values. A symmetrical square loop curve is observed in neutral media. In comparison, the curve shape is distorted in both acid and alkaline media, and the current gets much larger.

The square loop-shaped curve in neutral media indicates a mere charging/discharging process in the double layer, and negligible faradic process occurs on the surface in the investigated potential range. When the pH is 1, the curve is distorted, and several redox peaks are observed. Broad anodic peaks are found in the potential range of 0.4−0.9 V, which are associated with the cathodic peaks in the range of 0.9−0.4 V. These peaks are acknowledged to result from the oxidation/reduction of hydroquinone-/quinone-like groups in enriched chemical environments on the carbon surface.[28] Among these peaks, a pair of peaks with comparable currents are found at 0.656 and 0.592 V, respectively. This redox couple can be seen as electrochemically reversible, and the transition is accompanied by one-electron transfer per proton. Finally, it is noted that the peaks are considerably broad in width, indicating that the electron transfer process occurs on a variety of functional groups under enriched electronic environments. Similar to the case in acid, higher pseudocapacitant current is also observed in alkaline media. The broad peaks in the potential range of 0−0.8 V seem to be pretty symmetrical in curve shape, indicating fast electron transfer processes in this range.

Finally, it is noted that in all three electrolyte solutions, a continuous increase in the anodic current is seen above 1.1 V in the forward scan, which should be related to the "deep" electrochemical reaction of carbon. Another cathodic peak is found at 0−0.1 V in the reverse scan, which has not been fully understood yet and might be associated with the underpotential deposition of hydrogen.

3.2. Electrochemical Behavior at pH = 0, 1, 2. *3.2.1. CV and LSV.* Figure 2 shows the CV curves of the catalyst at pH = 0, 1, 2. It is seen that both the capacitance and pseudocapacitance currents increase with acid concentration, whereas the electrode potential of the redox peaks remains unchanged. This behavior can be understood as follows. First, the diffuse layer becomes more compact, and thus, the capacitance current gets increased as the electrolyte concentration rises. The same trend is also found when increasing the concentration of the supporting electrolyte (see Figure S2). Second, the reversible redox peaks at 0.6 V increase in current but remain unchanged in potential (vs RHE), which indicates that one electron per proton is directly involved in the electrochemical transition.

Figure 3 shows the corresponding RRDE results of the ORR in acid media. It is seen that the three polarization curves are basically overlapped in the investigated pH range. The generation of hydrogen peroxide coincides with the onset reduction of oxygen, and its yield is found to be lower than 6%.

The overlap of the polarization curves indicates that the proton, coupled with the first charge transfer, may participate in the rate-determining step (r.d.s.) of the ORR. The r.d.s. is supposed to be

$$* + O_2 + H^+ + e^- \rightarrow *-(HO_2)_{ads} \quad (4)$$

It is noted that there still exists a non-negligible difference in the polarization curves, especially at the lowest pH of 0. In other words, increasing the proton concentration yields a negative effect on the reaction kinetics. Another effect has to be considered to explain this phenomenon. It has been claimed that nitrogen-activated carbon atoms are the active sites for catalyzing the ORR, and the delocalized lone pair of electrons from the doped nitrogen atoms facilitates the charge transfer from π to the antibonding orbitals in dioxygen.[27] Here, we speculate that highly positively charged proton ions may strongly interact with the lone-pair electrons of the nitrogen atoms,[24,29] lowering the degree of the charge delocalization and, thus, the catalytic activity. Such an acid−base neutralization reaction is confirmed by the continuous increase in pH when immersing the catalyst into the acid solution (see Figure S3).

In addition, it is noted that the cathodic wave of the ORR is concomitantly overlapping with the reduction peak of the redox couple on the carbon surface. This intuitively indicates that the charge transfer to oxygen is mediated by the surface-confined redox couple on the carbon surface, which is further evidenced by the following Tafel analysis. As such, eq 4 can be rewritten as

$$Q + H^+ + e^- \leftrightarrow Q{-}H \quad (5)$$

$$Q{-}H + O_2 \rightarrow (Q{-}H{-}O_2)_{ads} \quad (6)$$

Finally, hydrogen peroxide is generated coincidentally when the oxygen reduction reaction starts to occur. This suggests that the subsequent proton transfer reaction competes in two ways,

DOI: 10.1021/acscatal.5b01089
ACS Catal. 2015, 5, 4325−4332

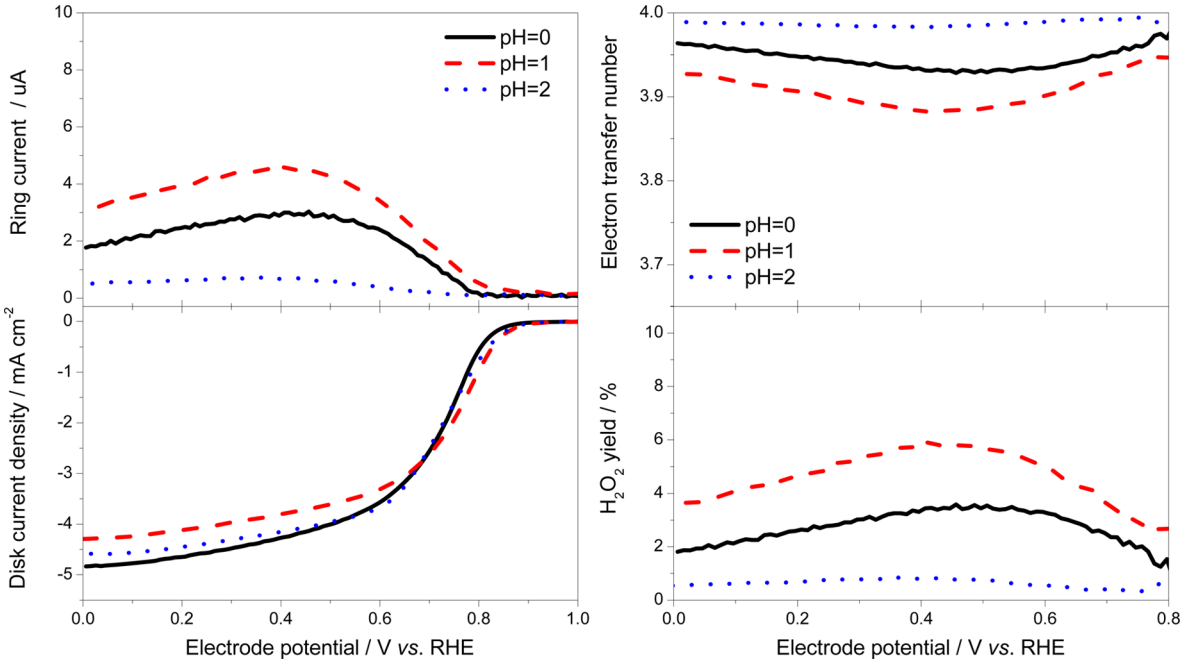

Figure 3. Rotating ring-disk polarization curves, peroxide yield and electron transfer number in oxygen-saturated $HClO_4$ solutions of three concentrations: 1.0, 0.10, and 0.010 M. Rotating rate, 1600 rpm; sweep rate, 5 mV s^{-1}.

which results in the parallel 2-e and 4-e reduction pathways. It is noted that the hydrogen peroxide yield is lower than 6%, and the calculated electron transfer number is ~4, revealing that the catalyst is selective to the 4-e reduction of oxygen in acid media. This feature is highly desirable for both the performance and stability of the catalyst in fuel cells.

Next, the mechanism is further investigated based on the Tafel analysis and reaction order of the proton.

3.2.2. Tafel Analysis and Reaction Order. From Figure 4, it is seen that the catalyst shows linear and parallel Tafel plots in acid media at high potentials (0.9−0.75 V), and the Tafel slope is found to be ~60 mV dec^{-1}. At lower potentials, the curves are bent downward and there is no well-defined linear region found in the plot. The parallel Tafel plot indicates that the r.d.s. remains the same when varying the pH in the range of 0−2.

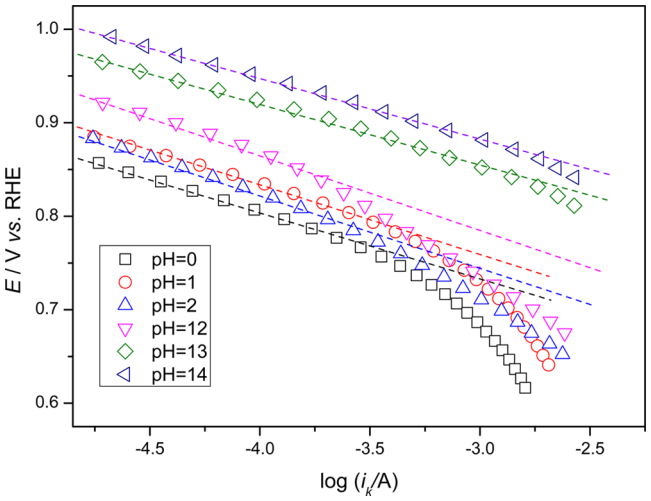

Figure 4. Tafel plot of the catalyst in oxygen-saturated electrolyte solutions. Here, the kinetics current (i_k) is extracted from the RDE results on the basis of the Koutecky−Levich equation.

The Nernstian slope (60 mV dec^{-1}) agrees with the speculation on the redox mediation mechanism (vide supra).[22,29]

In the above mechanism, the reaction order should be first for proton. Here, the reaction order of the proton $(((\partial \log i_k)/(\partial \log a_{H^+}))_E)$ can be obtained from

$$\left(\frac{\partial \log i_k}{\partial \log a_{H^+}}\right)_E = -\left(\frac{\partial \log i_k}{\partial E}\right)_{a_{H^+}}\left(\frac{\partial E}{\partial \log a_{H^+}}\right)_{i_k} \quad (7)$$

where the first term, $-((\partial \ln i_k)/(\partial E))_{a_{H^+}}$, is the reciprocal of Tafel slope, and the second term $((\partial E)/(\partial \log a_{H^+}))_{i_k}$ is 60 mV dec^{-1} (see Figure 3).

Accordingly, the reaction order of proton is, indeed, first. This simple calculation confirms the validity of the proposed redox-mediated mechanism, as described by eqs 5, 6.

3.3. Electrochemical Behavior at pH = 12, 13, 14.

3.3.1. CV and LSV. Figure 5 shows the cyclic voltammetry curves of the catalyst at pH = 12, 13, 14. Similar to the case in acid, the charging current increases with the KOH concentration, and the broad redox peak also remains unchanged in potential (see Figure S4). The redox peaks should result from the sorption of hydroxyl ions onto the carbon surface. The anodic/cathodic peaks of the OH sorption are basically symmetrical in shape, indicating that this process proceeds very quickly and reversibly.

$$* + OH^- \leftrightarrow *{-}OH_{ads} + e^- \quad (8)$$

$$*{-}OH_{ads} + OH^- \leftrightarrow *{=}O_{ads} + H_2O + e^- \quad (9)$$

Equations 8 and 9 correspond to a two-step charge-transfer process. Albeit undifferentiated, the former process should occur at lower potentials, and the latter one, at higher potentials. Accordingly, at higher potentials, such as above 0.9 V, the coverage of $-OH_{ads}$ (θ) can be written from eq 9 by assuming a Langmuir adsorption.

DOI: 10.1021/acscatal.5b01089
ACS Catal. 2015, 5, 4325−4332

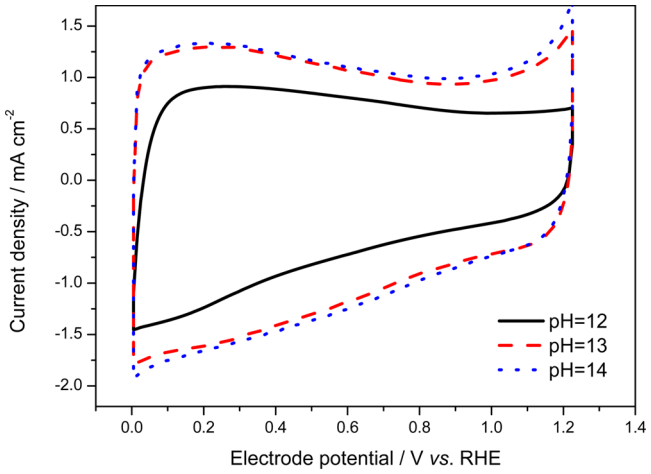

Figure 5. Cyclic voltammetry curves of the catalyst in KOH solutions of three concentrations: 1.0, 0.10, and 0.010 M.

$$\theta = \frac{1}{1 + a_{OH^-}\exp(F(E-E^0)/RT)} \quad (10)$$

where a_{OH^-} is the activity of OH^-, F is the faradic constant, R is the gas constant, T is the absolute temperature, E is the electrode potential, and E^0 is the equilibrium potential.

Figure 6 shows the corresponding polarization curves of the ORR at the three pHs. It is seen that increasing the KOH concentration yields a significant effect on the electrochemical behavior. First, the performance continues to be improved with increasing the KOH concentration. Second, the generation of hydrogen peroxide occurs at a much lower potential than the onset potential of the ORR. Finally, both the KOH concentration and the electrode potential have a significant effect on the yield of hydrogen peroxide, and the electron transfer number decreases from 4 to 3.3 when the KOH concentration increases from 0.010 to 1.0 M.

To understand the electrochemical performance, the mechanism of the ORR needs to be first considered. Generally, it is believed that oxygen has to be adsorbed onto the active sites before the successive charge transfer, namely, the innersphere electron transfer (ISET) mechanism.[3,10] However, it was recently suggested that the oxygen molecule is energetically unfavorable to being adsorbed onto the active sites.[19,20] Its solvated form at the outer-Helmholtz plane can draw one electron from the electrode by the tunneling effect, and the resultant oxygen radicals can be effectively adsorbed onto the nitrogen-doped sites.[19,20] Figure 6 shows the ORR occurs at a high onset potential, which falls within the potential range of eq 9. At this onset potential, it seems unreasonable to speculate that the enriched oxygenated species can be fully stripped off, leaving free carbon atoms for the oxygen adsorption. As such, the adsorption of oxygen should occur onto the active sites by hydrogen-bonding with $*-OH_{ads}$ species. The reaction is then written as eq 11, which is r.d.s. for the ORR in alkaline media at high potentials.

$$*-OH_{ads} + O_2 \rightarrow *-(OH-O_2)_{ads} \quad (11)$$

This mechanism is analogous to the aforementioned one in the acid media, and the first charge transfer is mediated by the reduced form of the surface-confined redox couple. On the basis of eqs 9−11, the kinetics equation can be derived as

$$i = 4Fk_{11}a_{O_2}\Gamma\frac{1}{1 + a_{OH^-}\exp(F(E-E^0)/RT)} \quad (12)$$

where i is the current density, k_{11} is the reaction constant, a_{O_2} is the activity of oxygen, and Γ is the saturated adsorption capacity.

Accordingly, the improvement in the polarization curve (vs RHE) can be qualitatively rationalized in terms of increasing

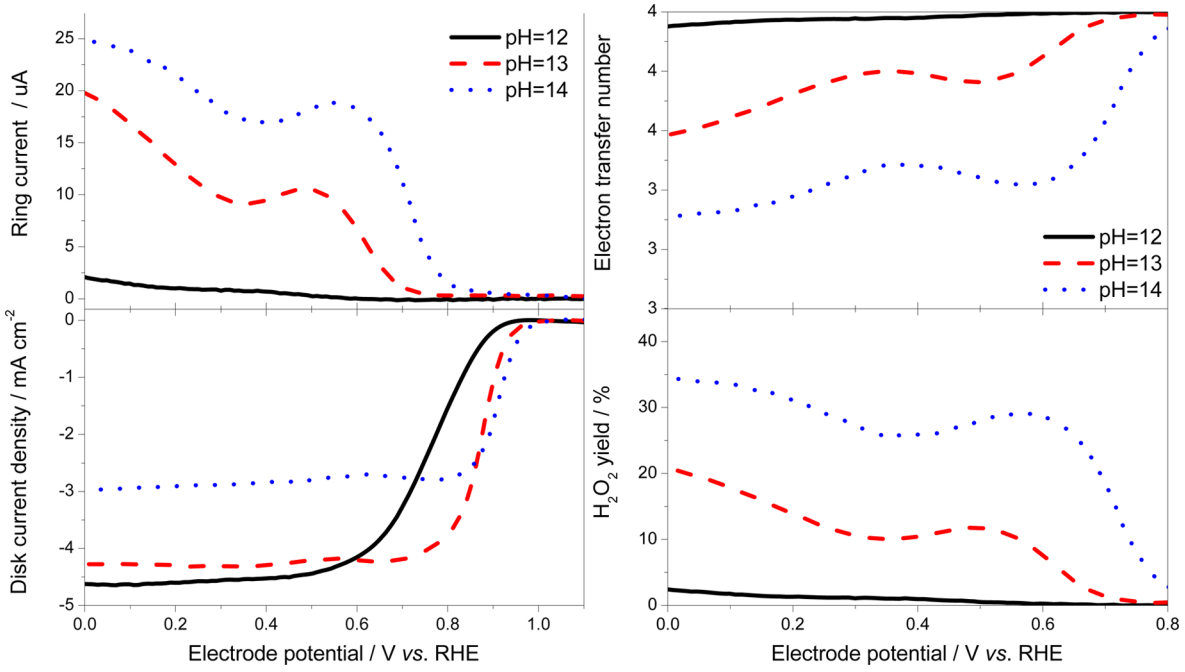

Figure 6. Rotating ring-disk polarization curves, peroxide yield, and electron transfer number in oxygen-saturated KOH solutions of three concentrations: 1.0, 0.10, and 0.010 M. Rotating rate, 1600 rpm; sweep rate, 5 mV s^{-1}.

DOI: 10.1021/acscatal.5b01089
ACS Catal. 2015, 5, 4325−4332

the KOH concentration. The kinetics equation agrees well with the Tafel analysis and reaction order, as discussed below.

Another finding is that the potential of generating hydrogen peroxide is much lower than that of the ORR, and the yield of hydrogen peroxide increases with decreasing potential and increasing KOH concentration. This result can be rationalized by considering steps to parallel eq 11. It is acknowledged that the generated superoxide radical remains stable in alkaline media, which may participate in the successive reactions in the following pathways:

(1) The radicals are adsorbed onto the active sites of the nitrogen-doped carbon catalyst, are stepwise-dissociated, and finally reduced to water by an innersphere electron transfer (ISET) mechanism.
(2) The solvated superoxide radicals remain stable and stay in the outer-Helmholtz plane, which then capture another electron and are protonated to yield hydrogen peroxide by an outersphere electron transfer (OSET) mechanism.

At high potentials, the absence of hydrogen peroxide indicates that the ORR predominantly proceeds in an ISET mechanism (see eq 11). With the decrease in potential (viz., work function), OSET is enhanced, and the ORR proceeds in a parallel mechanism.[30,31]

3.3.2. Tafel Analysis and Reaction Order. The Tafel plot in alkaline solution is shown in Figure 4. It is seen that the three plots show a linear and parallel region and the Tafel slope is 60−70 mV dec^{-1}. Accordingly, the reaction order of hydroxyl ions $((\partial \log i)/(\partial \log a_{OH^-}))_E$ is found to be ∼−0.5 at high potentials. The above findings can be qualitatively understood by eq 12. Discrepancies may exist as a result of the assumption of an ideal Langmuir adsorption. Such a self-consistency confirms that the r.d.s. (eq 11) is valid at high potentials.

3.4. LSV in Acid and Alkaline. Figure 7 shows the polarization curves of the carbon catalyst in both acid and alkaline solutions. A big gap is seen in the two polarization curves, and the catalyst shows a superior performance in alkaline media. Such a big difference is supposed to lie in the change of the active sites and their interaction with oxygen in the two media. At higher potentials, oxygen strongly interacts with the active sites on the surface, and its reduction proceeds in a redox-mediated mechanism. Therefore, the intrinsic activity depends on the chemical nature of the active sites.[23] It is acknowledged that the doped nitrogen atoms may experience a fast protonation process[24,29] and adsorption of anions,[26] degrading the electrocatalytic activity. In comparison, the doped nitrogen atoms do not participate in such a neutralization reaction in alkaline media. As a result, the lone pair electrons on the dopant nitrogen can be effectively shared by the adjacent active sites, favoring the charge transfer and the consequent reduction of oxygen. In additions, in alkaline media, the charge transfer may proceed by a parallel OSET mechanism without a strong interaction between oxygen and electrode.[19,20,23,32−34] Such a contribution cannot be fully excluded so far, which may further results in the better activity in alkaline media.

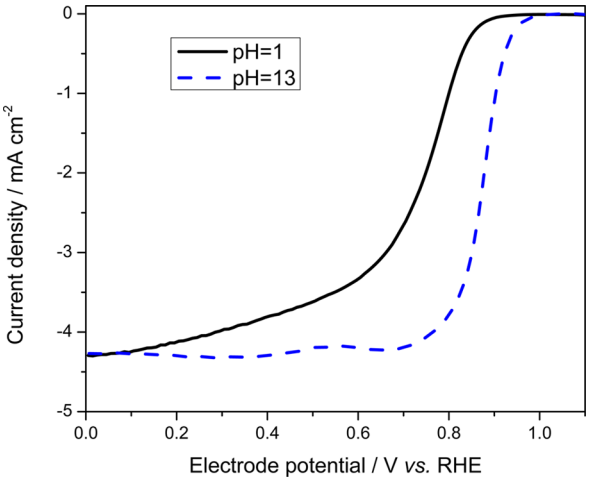

Figure 7. Rotating disk polarization curves in oxygen-saturated 0.10 M KOH and 0.10 $HClO_4$ solutions. Rotating rate, 1600 rpm; sweep rate, 5 mV s^{-1}.

3.5. Loop Behavior of the Polarization Curve. Figure 8 shows the positive-going and negative-going polarization loop curves of the carbon catalyst and platinum catalyst in both acid and alkaline media. For the platinum catalyst, it is seen that the polarization curve in the positive-going scan is much better than that in the negative-going one, leaving a hysteresis loop in the polarization curve. In comparison, such a hysteresis loop is not observed for the carbon catalyst in either acid or alkaline

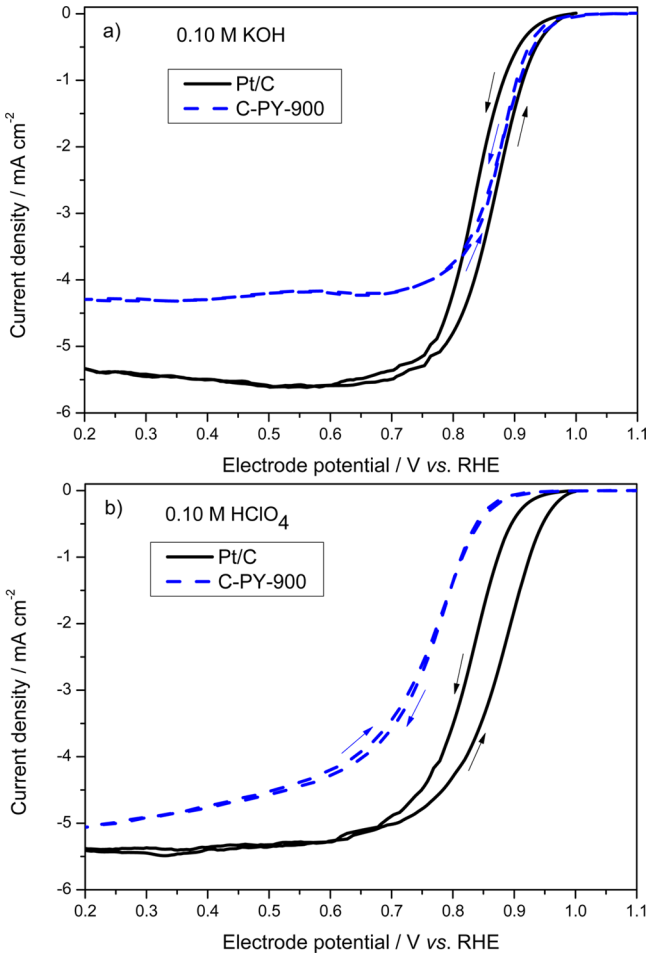

Figure 8. Rotating ring-disk polarization curves in oxygen-saturated: (a) 0.10 M KOH solution and (b) 0.10 M $HClO_4$ solution. Rotating rate, 1600 rpm; sweep rate, 5 mV s^{-1}; scanning potential region: 0−1.2 V for carbon, 0−1.0 V for Pt/C.

DOI: 10.1021/acscatal.5b01089
ACS Catal. 2015, 5, 4325−4332

media. Understanding of the surface processes is needed to clarify the behavior in collecting the cyclic polarization curves. For the Pt/C catalyst, it is acknowledged that the coverage of adsorbed surface oxide species has a pronounced effect on the ORR performance. Fully covered oxide species can retard the adsorption of oxygen and, thus, lower the ORR polarization curve.[35] Cyclic voltammetry reveals that the oxide species starts to form at potentials above 0.7 V in the positive-going scan and gets stripped off below 1.0 V in the negative-going scan. As a result, the oxide coverage gradually increases as the potential is positively scanned in the forward sweep and decreases in the backward scan. As such, the hysteresis loop in the cyclic polarization curve can be qualitatively understood by considering the coverage of the adsorbed oxide species. The case is different for the carbon catalyst. The ORR proceeds in a redox-mediated mechanism, in which the adsorbed surface species ($-OH_{ads}$) does not block the charge transfer but acts as the bridge to facilitate the charge transfer. As such, the hysteresis loop behavior is not observed in the carbon-based catalyst.

3.6. Oxygen Adsorption Behavior. To further support the above analysis, the adsorption of oxygen on the carbon catalyst was investigated in both acid and alkaline media. The cathodic stripping voltammetry of the preadsorbed oxygen is seen in Figure 9. A broad cathodic wave is observed as the background current in the two Ar-saturated solutions, corresponding to the reduction of the adsorbed species on the surface. The cathodic current is found to remain unchanged after the adsorption of oxygen. This finding strongly confirms that at higher potentials, the surface is fully covered by $*{=}O_{ads}$-like species (see eq 9), and the adsorption of oxygen can occur only on the active site in the reactive form like $*{-}OH_{ads}$ (see eq 11).

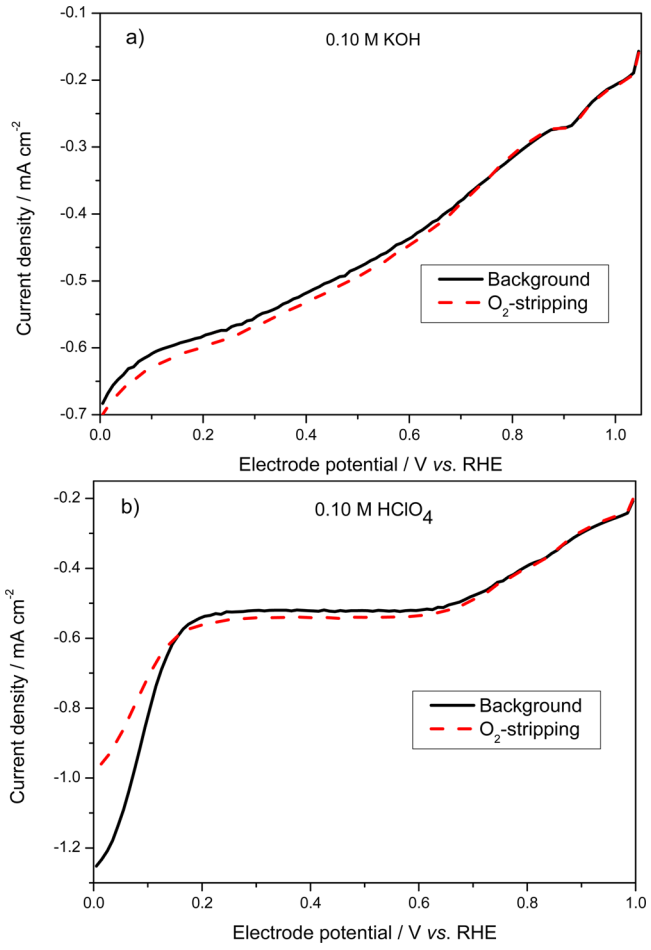

Figure 9. Cathodic stripping voltammetry of the preadsorbed oxygen on the carbon catalyst in the two solutions: (a) 0.10 M KOH,)b) 0.10 M $HClO_4$.

4. CONCLUSIONS

In this work, the effect of pH was extensively investigated on the nitrogen-doped carbon catalyst for the oxygen reduction reaction. It was found that the composition of the electrolyte solution yielded a considerable effect on the surface properties of the catalyst, the charge transfer in the double layer, and the electrochemical activity for the ORR. Salient findings are as follows: First, nitrogen-doped carbon shows a variety of functional groups with enriched reversible redox couples on the surface, acting as the bridge for the charge transfer to the adsorbed oxygen. Second, the mechanism of the ORR depends on the electrode potential and pH of the electrolyte solution. At high potentials, the ORR proceeds by a surface-confined redox-mediated catalysis mechanism, yielding a 4-e reduction reaction, in both acid and alkaline media. At lower potentials, a parallel charge transfer process by the outersphere electron transfer mechanism gets pronounced in alkaline media, yielding a considerable amount of hydrogen peroxide. Third, the nitrogen-doped carbon catalyst yields performance in alkaline media that is superior to that in acid media. Such a big gap in performance can be attributed to the change in the active sites and their interaction with oxygen in the two media. The protonation of doped nitrogen atoms hinders the charge delocalization and, thus, degrades its electrocatalytic activity in acid media. In conclusion, the chemical state of the functional groups is of paramount importance to determine the electrochemistry of nitrogen-doped carbon, and future work is needed to quantify their change with respect to the pH and electrode potential.

■ ASSOCIATED CONTENT

Supporting Information

The Supporting Information is available free of charge on the ACS Publications website at DOI: 10.1021/acscatal.5b01089.

Conditioning potentials for the oxygen-stripping voltammetry, effect of the KNO_3 concentration on cyclic voltammetry curves, effect of adding the carbon catalyst on the solution pH, effect of adding KNO_3 on CV and LSV (PDF)

■ AUTHOR INFORMATION

Corresponding Author

*Phone: +86 20 87113584. E-mail: zliang@scut.edu.cn.

Notes

The authors declare no competing financial interest.

■ ACKNOWLEDGMENTS

The work described in this paper was jointly supported by the Pearl River S&T Nova Program of Guangzhou (No. 2013J2200041), the National Natural Science Foundation of China (Nos. 21476087, 21003052), the Innovation Project of Guangdong Department of Education (No. 2014KTSCX016),

DOI: 10.1021/acscatal.5b01089
ACS Catal. 2015, 5, 4325−4332

and Guangdong Natural Science Foundation (No. S2013010012469).

REFERENCES

(1) Bashyam, R.; Zelenay, P. *Nature* **2006**, *443*, 63.
(2) Jasinski, R. *Nature* **1964**, *201*, 1212.
(3) Gong, K. P.; Du, F.; Xia, Z. H.; Durstock, M.; Dai, L. M. *Science* **2009**, *323*, 760.
(4) Lefevre, M.; Proietti, E.; Jaouen, F.; Dodelet, J. P. *Science* **2009**, *324*, 71.
(5) Wu, G.; More, K. L.; Johnston, C. M.; Zelenay, P. *Science* **2011**, *332*, 443.
(6) Zhou, X. J.; Qiao, J. L.; Yang, L.; Zhang, J. J. *Adv. Energy Mater.* **2014**, *4*, 25.
(7) Zhao, A.; Masa, J.; Xia, W.; Maljusch, A.; Willinger, M. G.; Clavel, G.; Xie, K.; Schloegl, R.; Schuhmann, W.; Muhler, M. *J. Am. Chem. Soc.* **2014**, *136*, 7551.
(8) Zhang, W.; Wu, Z. Y.; Jiang, H. L.; Yu, S. H. *J. Am. Chem. Soc.* **2014**, *135*, 14385.
(9) Zhang, P.; Sun, F.; Xiang, Z. H.; Shen, Z. G.; Yun, J.; Cao, D. P. *Energy Environ. Sci.* **2014**, *7*, 442.
(10) Xiang, Z.; Xue, Y.; Cao, D.; Huang, L.; Chen, J. F.; Dai, L. *Angew. Chem., Int. Ed.* **2014**, *53*, 2433.
(11) Wen, Z.; Ci, S.; Hou, Y.; Chen, J. *Angew. Chem., Int. Ed.* **2014**, *53*, 6496.
(12) Wang, M. Q.; Yang, W. H.; Wang, H. H.; Chen, C.; Zhou, Z. Y.; Sun, S. G. *ACS Catal.* **2014**, *4*, 3928.
(13) Park, J.; Nabae, Y.; Hayakawa, T.; Kakimoto, M. A. *ACS Catal.* **2014**, *4*, 3749.
(14) Deng, D. H.; Pan, X. L.; Yu, L. A.; Cui, Y.; Jiang, Y. P.; Qi, J.; Li, W. X.; Fu, Q. A.; Ma, X. C.; Xue, Q. K.; Sun, G. Q.; Bao, X. H. *Chem. Mater.* **2011**, *23*, 1188.
(15) Li, Y. G.; Zhou, W.; Wang, H. L.; Xie, L. M.; Liang, Y. Y.; Wei, F.; Idrobo, J. C.; Pennycook, S. J.; Dai, H. J. *Nat. Nanotechnol.* **2012**, *7*, 394.
(16) Proietti, E.; Jaouen, F.; Lefevre, M.; Larouche, N.; Tian, J.; Herranz, J.; Dodelet, J. P. *Nat. Commun.* **2011**, *2*, 416.
(17) Yu, D. S.; Zhang, Q.; Dai, L. M. *J. Am. Chem. Soc.* **2010**, *132*, 15127.
(18) Qu, L. T.; Liu, Y.; Baek, J. B.; Dai, L. M. *ACS Nano* **2010**, *4*, 1321.
(19) Choi, C. H.; Lim, H. K.; Chung, M. W.; Park, J. C.; Shin, H.; Kim, H.; Woo, S. I. *J. Am. Chem. Soc.* **2014**, *136*, 9070.
(20) Ramaswamy, N.; Tylus, U.; Jia, Q.; Mukerjee, S. *J. Am. Chem. Soc.* **2013**, *135*, 15443.
(21) Liang, Y. Y.; Li, Y. G.; Wang, H. L.; Zhou, J. G.; Wang, J.; Regier, T.; Dai, H. J. *Nat. Mater.* **2011**, *10*, 780.
(22) Tylus, U.; Jia, Q.; Strickland, K.; Ramaswamy, N.; Serov, A.; Atanassov, P.; Mukerjee, S. *J. Phys. Chem. C* **2014**, *118*, 8999.
(23) Li, Q. Q.; Noffke, B. W.; Wang, Y. L.; Menezes, B.; Peters, D. G.; Raghavachari, K.; Li, L. S. *J. Am. Chem. Soc.* **2014**, *136*, 3358.
(24) Li, X. G.; Liu, G.; Popov, B. N. *J. Power Sources* **2010**, *195*, 6373.
(25) Meng, H.; Jaouen, F.; Proietti, E.; Lefevre, M.; Dodelet, J. P. *Electrochem. Commun.* **2009**, *11*, 1986.
(26) Herranz, J.; Jaouen, F.; Lefevre, M.; Kramm, U. I.; Proietti, E.; Dodelet, J. P.; Bogdanoff, P.; Fiechter, S.; Abs-Wurmbach, I.; Bertrand, P.; Arruda, T. M.; Mukerjee, S. *J. Phys. Chem. C* **2011**, *115*, 16087.
(27) Wan, K.; Long, G. F.; Liu, M. Y.; Du, L.; Liang, Z. X.; Tsiakaras, P. *Appl. Catal., B* **2015**, *165*, 566.
(28) Blurton, K. F. *Electrochim. Acta* **1973**, *18*, 869.
(29) Gouérec, P.; Biloul, A.; Contamin, O.; Scarbeck, G.; Savy, M.; Riga, J.; Weng, L. T.; Bertrand, P. *J. Electroanal. Chem.* **1997**, *422*, 61.
(30) Gattrell, M.; MacDougall, B. In *Handbook of Fuel Cells*; John Wiley & Sons, Ltd: New York, 2010.
(31) Ross, P. N. In *Handbook of Fuel Cells*; John Wiley & Sons, Ltd: New York, 2010.
(32) Xing, T.; Zheng, Y.; Li, L. H.; Cowie, B. C. C.; Gunzelmann, D.; Qiao, S. Z.; Huang, S. M.; Chen, Y. *ACS Nano* **2014**, *8*, 6856.
(33) Wang, Q.; Zhou, Z. Y.; Lai, Y. J.; You, Y.; Liu, J. G.; Wu, X. L.; Terefe, E.; Chen, C.; Song, L.; Rauf, M.; Tian, N.; Sun, S. G. *J. Am. Chem. Soc.* **2014**, *136*, 10882.
(34) Wiggins-Camacho, J. D.; Stevenson, K. J. *J. Phys. Chem. C* **2011**, *115*, 20002.
(35) Gasteiger, H. A.; Ross, P. N. *J. Phys. Chem.* **1996**, *100*, 6715.

DOI: 10.1021/acscatal.5b01089
ACS Catal. 2015, 5, 4325−4332